Formation and Photolability of Low-Spin Ferrous Cytochrome *c* Peroxidase at Alkaline pH†

Jianling Wang, Nancy J. Boldt, and Mark R. Ondrias*

Department of Chemistry, University of New Mexico, Albuquerque, New Mexico 87131

Received June 14, 1991; Revised Manuscript Received October 10, 1991

ABSTRACT: The ferrous form of native cytochrome *c* peroxidase (CCP) is known to undergo a reversible transition when titrated over the pH range of 7.00–9.70. This transition produces a conversion from a pentacoordinate high-spin to a hexacoordinate low-spin heme active site and is clearly apparent in the heme optical absorption spectra. Here, we report the characterization of this transition and its effect upon the local heme environment using various optical spectroscopies. The formation of hexacoordinate low-spin heme is interpreted to involve the binding of His-52 at the distal site after the perturbation of the extensive H-bonded network within and around the heme pocket of CCP(II) at alkaline pH. Interestingly, CD investigations of CCP(II) in the far-UV and Soret regions indicate the dissappearance of a single high-spin species and the existence of at least two low-spin species of CCP(II) as the pH is raised above 7.90. Furthermore, transient resonance Raman experiments demonstrate that the hexacoordinate low-spin species can be photolyzed within 10-ns laser pulses, producing a species similar to the low-pH (high-spin) form of CCP(II) at alkaline pH. However, the extent of photolysis is quite pH dependent, with a maximum photodissociation yield at pH = 8.50.

Cytochrome *c* peroxidase (CCP), a mitochondrial heme protein of yeast (Yonenati, 1970, 1976; Poulos & Finzel, 1984) catalyzes the oxidation of ferrocytochrome *c* to ferricytochrome *c* and the reduction of hydrogen peroxide to water. This protein is an example of a catalytic heme protein where the protein matrix plays a direct role in the functional mechanism of the active site. In addition to providing the fifth ligand (His-175) for the heme active site and creating an environment which accommodates the heme's low redox potential (−190 mV), the protein matrix also supplies specific amino acids necessary to stabilize the energetically unfavorable charge separation of RO–OH substrate in the activated complex (Poulos & Finzel, 1984). Peroxidase catalysis is believed to follow a mechanism which includes (1) directed proton transfer or acid–base catalysis by His-52 in the distal heme pocket; (2) stabilization of negative charge on the peroxide oxygens by Arg-48; (3) stabilization of a ferryl iron by the proximal histidine; and (4) the creation of an organic radical by Trp-191 in the proximal site (Goodin et al., 1987; Erman et al., 1989; Sivaraja et al., 1989) and probably a second-radical migration pathway (Tsaprailis et al., 1991).

The mechanism of CCP function has been inferred largely from the relatively well-known equilibrium structure of its active site. High-resolution crystal structures show that the heme in CCP is held in a crevice between two antiparallel helices, by a rigid network of hydrogen bonds. In the resting enzyme, the Fe atom is out of the heme plane on the proximal side as a result of bonding to the His-175 residue. A nonbonding water molecule resides on the distal side of the heme (Poulos et al., 1980; Poulos, 1982). The hydrogen-bonding network on the proximal side involves the multiple bonds of Asp-235 with His-175, Trp-191, and H_2O-535. On the distal side, it has been postulated that H_2O-595 (the axial water ligand) hydrogen bonds with His-52 and Trp-51. This network of hydrogen bonds likely includes the bonding of H_2O-548···Arg-48···H_2O-348, forming a distal ligation pocket which is accessible to the peroxide, other external ligands (F^-, Cl^-, CN^-, CO, NO, imidazole, etc.), and solvent molecules (PO_4^{3-}, etc.) via a channel connecting the distal side of the heme crevice with the protein surface. The edge of pyrrole IV lies at the frontier of the channel about 10 Å from the molecular surface, and only Trp-51 of those distal side residues is really buried.

A knowledge of the structural dynamics of this heme pocket active site is essential in order to completely characterize the functional mechanism of CCP. This is particularly relevant since the CCP heme pocket is quite susceptible to environmental perturbations. For instance, CCP is believed to exist in either an acidic form or an alkaline form (Yonenati, 1970). Previous physical studies have already provided considerable insight into the pH-dependent structural changes in CCP. For instance, EPR spectra of CCP(III) display the signals typical of high-spin heme iron at pH = 5.0 and the formation of low-spin heme iron (~60%) at pH = 8.4 (Wittenberg et al., 1968). Optical absorption studies on CCP(III) show a complex set of spectral transitions with increasing pH, while those of ferrous CCP clearly exhibit a high-spin heme at low pH and a low-spin heme at high pH with an apparent pK_a of 7.7 (Conroy et al., 1978). A better understanding of the nature of the transition between the two forms is extremely useful in the interpretation of the functional mechanism of CCP.

Resonance Raman spectroscopy has proven to be a powerful technique for the determination of biostructures and mechanisms (Spiro, 1987). Extensive studies have been carried out on cytochrome *c* peroxidase by this technique (Felton et al., 1976; Sievers et al., 1979; Shelnutt et al., 1983; Evangelista-Kirkup et al., 1985; Hashimoto et al., 1986; Smulevich et al., 1986a–c, 1988a,b, 1989a,b, 1990; Dasgupta et al., 1989; Reczek et al., 1989; Spiro et al., 1990; Wang et al., 1990, 1991). Previous resonance Raman studies of the pH dependence of CCP focused on the equilibrium forms of the enzyme (Shelnutt et al., 1983; Hashimoto et al., 1986; Smulevich et al., 1988a; Dasgupta et al., 1989). At pH 4.3–7.0, CCP(III) exhibits a pentacoordinate high-spin heme in fresh protein.

† This work was supported by the NIH (GM33330).

* To whom correspondence should be addressed.

0006-2960/92/0431-867$03.00/0

For the aged enzyme, a pH-dependent transition between penta- and hexacoordinate high-spin species, $pK_a = 5.5$, was observed (Dasgupta et al., 1989). The hexacoordinate low-spin heme observed in the alkaline pH matrix was believed to be due to the ionization and consequent binding of distal histidine-52 at the sixth ligand site, $pK_a = 7.6$ (Shelnutt et al., 1983; Hashimoto et al., 1986). The equilibrium form of CCP(II) has been reported as being both high spin (Hashimoto et al., 1986; Smulevich et al., 1988a; Dasgupta et al., 1989) and low spin at alkaline pH (Conroy et al., 1978; Smulevich et al., 1989b; Spiro et al., 1990; Miller et al., 1990; Wang et al., 1991). Recently, Spiro and co-workers (Smulevich et al., 1989b; Spiro et al., 1990) revealed the presence of photolabile low-spin heme within CCP(MI) at high pH.

This work expands upon previous studies by using steady-state and transient resonance Raman spectroscopy to characterize the pH-dependent equilibrium and dynamic behavior of the CCP(II) heme pocket. The information obtained via circular dichroism (CD) and optical absorption studies nicely complements the resonance Raman data. In particular, CD offers another powerful tool for investigating both the local heme environment and the overall secondary and tertiary structure of heme proteins (Myer & Pande, 1976; Myer, 1985; Woody, 1985).

Materials and Methods

Twice-crystallized cytochrome *c* peroxidase was isolated and purified from commercial baker's yeast (Red Star) by a modification of the procedure (Kang et al., 1977) of Yonetani and Nelson et al. (1977), developed by Moench (1986). Freshly prepared cytochrome *c* peroxidase was employed for all the optical absorption, CD, and resonance Raman experiments to guard against the possible structural and spectral changes induced by the aging of the protein (Dasgupta et al., 1989). The concentration of ferric cytochrome *c* peroxidase was spectroscopically determined at 408 nm, using an extinction coefficient of 93 mM^{-1} cm^{-1} (Yonetani & Ray, 1965). Ferric samples of cytochrome *c* peroxidase were obtained by directly dissolving CCP crystals into the buffer (100 mM Mes or Tris-HCl) solutions with different pH values as required. Ferrous cytochrome *c* peroxidase (~100 μM) was prepared by degassing a solution of the ferric enzyme with five cycles of vacuum/N_2, followed by the addition of several grains of solid sodium dithionite under completely anaerobic conditions. All the samples were checked after spectroscopy to ensure that sample preparation produced no unanticipated changes in pH. Care was excised to use only fresh enzyme (i.e., samples where the ferric enzyme was fully pentacoordinate and high spin at pH 7.30) in these investigations and to avoid the use of phosphate buffers.

Resonance Raman data were collected by instrumentation described in detail elsewhere, consisting of a nitrogen-pumped dye laser (Molectron UV-24/DL14), a SPEX 1430 double monochromator, and a SPEX DM3000R controller (Larsen, 1990). All the transient resonance Raman spectra were recorded, using 10-ns pulses, with 436-nm excitation. This wavelength is close to the isosbestic point of the Soret bands for low-spin (at 428 nm) and high-spin (at 440 nm) species of ferrous cytochrome *c* peroxidase. Raman spectra were calibrated by comparison with the well-known bands of benzene. During the measurements, the sample cell was cooled to approximately 4 °C by blowing cold dry nitrogen gas over the sample cell. Laser flux at the sample was regulated using focusing optics and/or neutral density filters to attenuate the beam. In this context, "high flux" refers to spherical focusing optics which yielded a flux of 1×10^8 W/cm^2 at the sample, while "low-flux" spectra were obtained using cylindrical optics and/or neutral density filters yielding $(3-8) \times 10^6$ W/cm^2 at the samples. Optical absorption spectra were obtained on a Hewlett-Packard HP8452A diode array UV/vis spectrometer. Circular dichroism experiments were carried out on a JASCO J-600 spectropolarimeter, at a scan speed of 10 nm/min. All the optical measurements were performed under the same experimental circumstances as those used for the transient resonance Raman investigations.

Spectra were deconvoluted as follows: The baseline was adjusted using a two-point linear correction. The spectra were then deconvoluted into Lorentzian bands that were allowed to vary in line width, position, and intensity in order to minimize χ-square values. The initial positions and line widths were estimated from assignments of known hexacoordinate low-spin and pentacoordinate high-spin protoheme bands (Spiro, 1982). Reasonable convergence was reached in less than 20 iterations. The adequacy of the fits was evaluated by subtracting the simulated from the real spectra. χ-square values of less than 0.04 were considered acceptable. For the isolated bands (e.g., ν_3), the curve fits allow quantitative comparison between the two species. In the more complicated regions (e.g., 1520–1650 cm^{-1}), however, the fits do not represent unique solutions but do allow the qualitative comparison of the relative contributions and the reasonable assignments of the band position.

Results

Characterization of CCP(II) by Absorption and RRS. Yeast cytochrome *c* peroxidase undergoes extensive structural modification upon exposure to high-pH media (>7.5) (Dowe & Erman, 1985). To further characterize this process and its effects on the heme active site, the titration of ferrous CCP was monitored by resonance Raman and optical absorption spectroscopy in the pH range from 7.30 to 9.70. The major effect of elevated pH on the absorption profile is a conversion of the heme to a low-spin configuration (see Figure 1). In Figure 1A, Soret bands at 426 nm (dotted line) and at 440 nm (solid line) indicate the presence of low-spin (pH = 9.70) and high-spin (pH = 7.30) hemes, respectively. Ferrous peroxidase equilibrated at pH = 8.50 exhibits a Soret band (428 nm) intermediate between the two extremes but more similar to that of low-spin heme. As the pH is raised further (to pH 9.70), the Soret extinction coefficient increases significantly (~36%). This process is also evident (Figure 1B) in the gradual increase in Q-band absorption for low-spin heme (528 nm and 558 nm) and a concomitant decrease in signal of high-spin species (588 nm). It is noteworthy that this is a kinetically slow process. Absorption spectra as a function of time subsequent to the anaerobic reduction of CCP are shown in Figure 1C,D. Equilibrium is achieved within 1–2 h after the reduction, depending, of course, on the temperature. In the present work, all the spectroscopic data were recorded only after equilibrium was reached.

Resonance Raman measurements of alkaline ferrocytochrome *c* peroxidase (Figure 2A) obtained at low laser flux were consistent with optical absorption data (Figure 1A,B). Scattering from both high-spin and low-spin hemes is enhanced with approximately equal magnitude in our resonance Raman spectra since the excitation wavelength (436 nm) is close to the isosbestic point of the Soret bands (434 nm) for the two spin states. The spectrum of imidazole-bound ferrocytochrome *c* peroxidase (Figure 2A, spectrum e) recorded at neutral pH serves as a reference for hexacoordinate low-spin heme. It shows ν_4 at 1361 cm^{-1}, a single ν_3 band at 1495 cm^{-1}, ν_{11} at 1559 cm^{-1}, ν_2 at 1584 cm^{-1}, ν_{37} at 1607 cm^{-1},

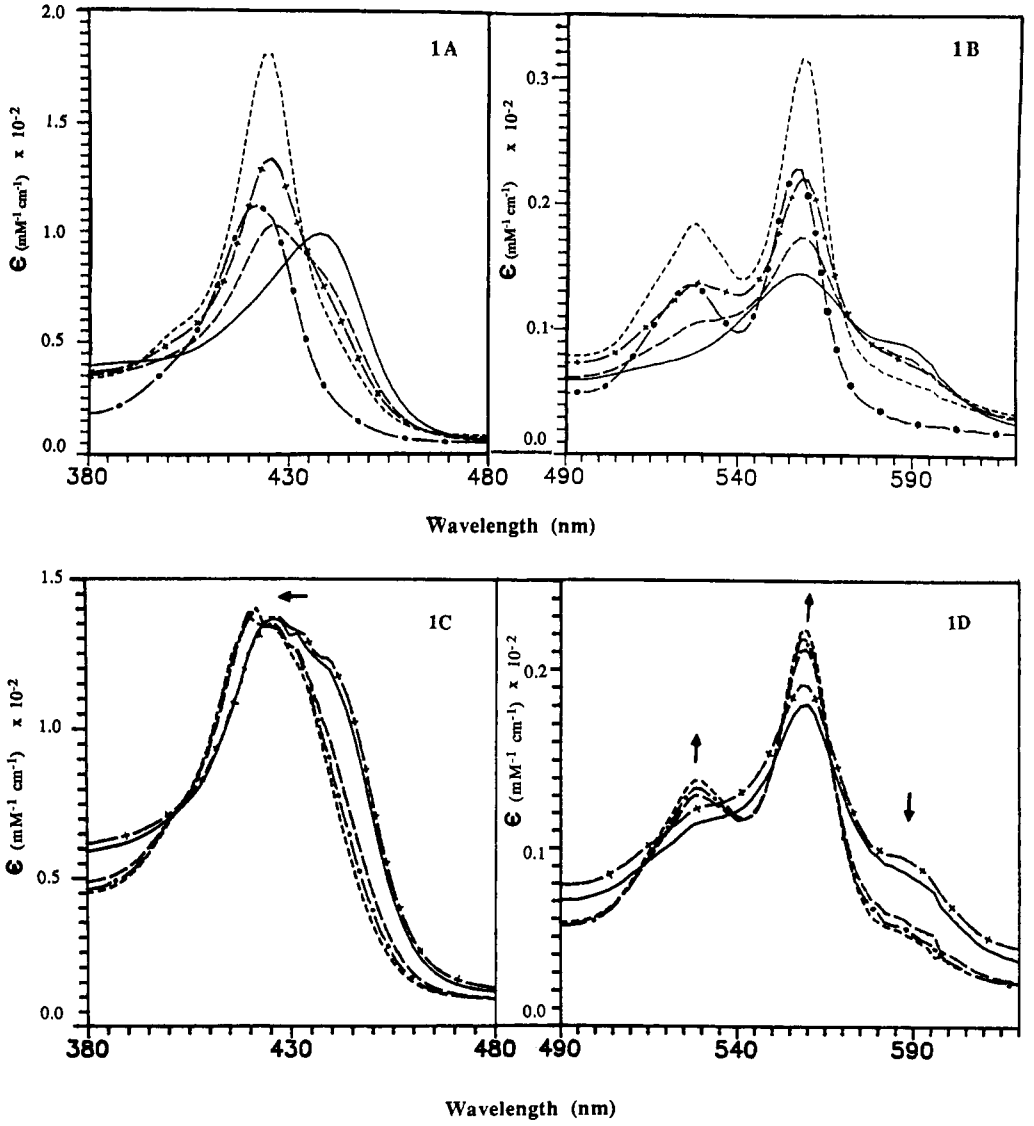

FIGURE 1: Optical absorption spectrum of fresh cytochrome *c* peroxidase (II) and its imidazole-bound derivative at different pHs in the Soret (A) and visible (B) regions: (—) CCP(II) at pH = 7.30; (– –) CCP(II) at pH = 7.90; (–+–) CCP(II) at pH = 8.50; (- - -) CCP(II) at pH = 9.70; (–·–) CCP(II)–Imd (1:1) at pH = 7.30. (C and D) Absorption spectra of CCP(II) at pH = 8.50, as a function of time subsequent to its anaerobic reduction: (—) immediately after reduction; (–+–) 20 min; (– –) 40 min; (–·–) 60 min; (- - -) 70 min after reduction. A 100 mM Tris-HCl buffer was used. Arrows indicate increasing time.

ν_{10} at 1620 cm^{-1}, and a vinyl mode at 1627 cm^{-1}. In contrast, ferrous CCP at pH 7.30 (Figure 2A, spectrum a) exhibits ν_4 at 1356 cm^{-1}, ν_3 at 1471 cm^{-1}, ν_{11} at 1551 cm^{-1}, ν_2 at 1563 cm^{-1}, ν_{37} at 1582 cm^{-1}, and ν_{10} at 1604 cm^{-1} as well as a vinyl stretching mode at 1618 cm^{-1}. These values are consistent with a pentacoordinate high-spin configuration (Spiro, 1983). The spectrum, however, varies markedly when the pH is raised from 7.30 to 9.70 (Figure 2A, spectrum d). The position of ν_4 (1360 cm^{-1}) and the presence of the two components of ν_3 (1471 cm^{-1} and 1495 cm^{-1}) suggest the existence of both the pentacoordinate high-spin and hexacoordinate low-spin heme structures. Furthermore, ν_{11} at 1558 cm^{-1}, ν_2 at 1581 cm^{-1}, ν_{37} at 1604 cm^{-1}, and ν_{10} at 1620 cm^{-1} as well as ν_{vinyl} at 1628 cm^{-1} are present. These are similar to those of imidazole-bound ferrous CCP obtained at neutral pH (Figure 2A, spectrum e). In accordance with the optical absorption results, ferrous CCP at pH = 8.50 (low laser flux) produces a resonance Raman spectrum in the high-frequency region similar to that at pH = 9.70 except for minor intensity changes in the ν_3 and ν_2 regions.

Spectra of ferrous CCP at pH > 7.60 could be reasonably modeled as the mixtures of pentacoordinate high-spin and hexacoordinate low-spin bands by (1) convolution of spectra of native ferrous CCP at pH = 7.30 (pentacoordinate/high spin; 5 c/hs) c/hs) and imidazole-bound ferrous CCP (hexacoordinate/low spin; 6 c/ls) (see Figure 3E) or (2) Lorentzian deconvolution of the individual spectra (see Figure 3A,D). Reasonable assignments of the high-frequency modes could be made and are summarized in Table I. These are largely consistent with assignments from previous investigations of the protoheme proteins (Spiro, 1982).

pH Titration of Alkaline CCP(II) by RRS. A pH titration of ferrous CCP (Figure 2B) was monitored by resonance Raman spectroscopy in order to quantify the spin-state and coordination transition. Since the position of ν_3 has been shown to be a more sensitive indicator of ligation state than the behavior of the other high-frequency modes (Dasgupta et al., 1989; Spiro et al., 1990) and it is well isolated from other high-frequency bands, it provides a better quantitative measurement of the pH-induced transitions of ferrous CCP. Spectra of CCP(II) obtained at low laser flux were recorded in the ν_3 region at different pHs. These are depicted in Figure 4A–C (lower panels) for pH = 9.70, 8.50, and 7.60, respectively. Obviously, the signal at 1495 cm^{-1}, corresponding to

Table I: Resonance Raman, Optical Absorption, and Circular Dichroism Data of Ferrous CCP under Different Conditions

	CCP(II)/X$^{-a,f}$		CCP(II),[b]	CCP(II), pH = 6.0		CCP(II),[a]	CCP(II),[d]	CCP(II),[d]	CCP(II),[a] pH = 8.50		CCP(II),[c]	CCP(II),[a]	CCP(II),[c]
	X = Imd	X = CN$^-$	pH = 5.0	*c*	*e*	pH = 7.30	pH = 7.80	pH = 8.44	low flux	high flux	pH = 8.55	pH = 9.70	pH = 10.5
Raman shift (cm^{-1})													
ν_4	1361	1360	1355			1356		1359	1360	1359		1360	
ν_3	1494	1495	1472			1471		1471/1493	1471/1495	1471/1495		1495	
ν_{11}	1559	1557				1551			1560	1556		1558	
ν_2	1584	1580	1565			1563			1583	1581		1581	
ν_{37}	~1607	1605				1582			1606	1603		1604	
ν_{10}	~1620	1618				1604			~1620	1619		~1620	
$\nu_{C=C}$	1627	1629	1617			1618			~1629	1627		~1628	
absorption[g] (nm)													
Soret	424 (112)	426 (120)		438 (~92)	439 (~110)	440 (97)	~426/~438	~424 (~140)	428 (132)		426 (~125)	426 (180)	~426 (~142)
β	528 (13.5)	532 (19)		559 (~13)	560 (~16)	558 (14)	~530/~561	530 (~12)	530 (13.5)		530 (~10)	528 (18)	~530 (~9)
α	556 (22.5)	562 (23.5)		~590 (~7.5)	589 (~10)	588 (9)	~561/590	561 (~21)	559 (22)		562 (~15)	558 (31)	~562 (~14)
CD[h] (nm)													
far UV						197 (+37)			199 (+13)			199 (+13)	
						210 (−190)			211 (−270)			213 (−300)	
						220 (−160)			221 (−233)			222 (−260)	
near UV					263 (+4)	262 (+1.62)			253 (+0.31)			256 (+0.15)	
					297 (−3.5)	288 (−2.85)			280 (−3.38)			275 (−3.54)	
						300 (−5.61)			299 (−3.54)			299 (−3.23)	
Soret	428 (−6.03)	432 (−17.3)			439 (−16)	443 (−13.4)			430 (−8.96)			429 (−11.73)	
γ	523 (−0.55)					524 (−1.18)			528 (−1.05)		528 (−0.93)		
β	537 (−0.76)				559 (−2)	560 (−1.82)			540 (−1.13)			540 (−1.18)	
α	558 (−1.18)				585 (−1.4)	590 (−1.22)			557 (−1.40)			557 (−1.59)	

[a] This work. [b] Dasgupta et al. (1989). [c] Conroy et al. (1978). [d] Smulevich et al. (1989b). [e] Sievers (1978). [f] Wang et al. (1991). [g] Data in parentheses are the corresponding extinction coefficients (mM^{-1} cm^{-1}). [h] Data in parentheses are the corresponding ellipticities (×10^4 deg cm^2/dmol).

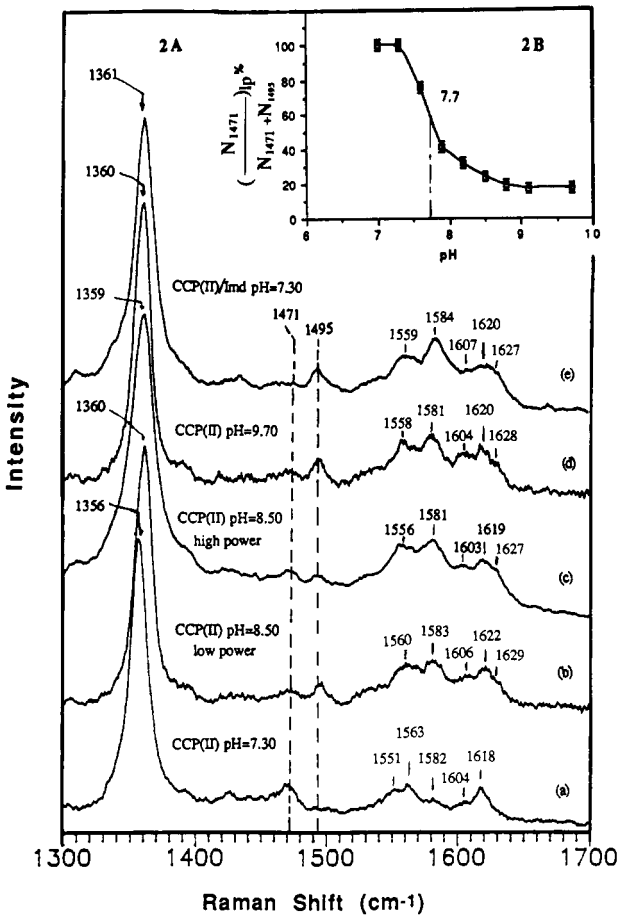

FIGURE 2: (A) Resonance Raman spectra of fresh cytochrome *c* peroxidase (II) and its imidazole derivative in high-frequency region: (a) CCP(II) at pH = 7.30; (b–c) CCP(II) at pH = 8.50; (d) CCP(II) at pH = 9.70; (e) CCP(II)–Imd (1:1) at pH = 7.30. All the spectra were obtained at low laser flux except (c). A 100 mM Tris-HCl buffer was used for CCP(II) and CCP(II)–Imd. The spectra are sums of 4–6 scans recorded at 10 cm^{-1}/min, with a cylindrical optics and 0.4-OD neutral density filter over 7 mW of average power. Excitation wavelength was 436 nm for measurements on CCP(II) and its imidazole-bound derivative. (B) High spin (ν_3 at 1471 cm^{-1}) to low spin (ν_3 at 1495 cm^{-1}) transition of CCP(II) expressed by the fractional population change of high-spin heme (see text for details).

the low-spin heme, is more predominant at pH = 9.70 (Figure 3A) than at pH = 7.60 (Figure 3C).

The peak area for each component was calculated from computer simulations of the observed spectra. In order to convert the areas of the two bands into relative populations of the hexacoordinate low-spin and pentacoordinate high-spin species, it was necessary to determine the relative cross-sections of ν_3 for these species. This was accomplished by obtaining spectra of ferrous CCP at pH = 7.30 (~100% pentacoordinate high spin) and its imidazole-bound derivative at pH = 7.30 (~100% hexacoordinate low spin) in the presence of 10% (w/v) $(NH_4)_2SO_4$. After the correction for reabsorption effects, the band of $(NH_4)_2SO_4$ at 981 cm^{-1} served as an internal intensity standard. It was found that the cross-section of ν_3 (excited at 436 nm, using 100 μM solutions of ferrous CCP) for the pentacoordinate high-spin species was 1.75 times that of the hexacoordinate low-spin species. The ratio of the relative population of high-spin species vs the sum of both high- and low-spin species was then plotted as a function of pH (Figure 2B). It appears that the transition from pentacoordinate high spin to hexacoordinate low spin is initiated at pH = 7.30 and is mostly completed at pH = 9.10. The pK_a for this transformation was estimated to be about 7.70 ± 0.10. This is close to the pK_a (7.60 ± 0.1) observed with optical titrations (Conroy et al., 1978). The plot of the percent of high spin vs pH is, however, asymmetric, perhaps indicating a second ionization at higher pH.

Circular Dichroism Experiments. The circular dichroism (CD) spectra of ferrocytochrome *c* peroxidase observed from 190 to 620 nm are shown in Figures 5 and 6. The high spin to low spin transition can also be detected from the CD spectra of native CCP(II) in the near-UV wavelength region (240–380 nm, Figure 5B). The optical activity of heme proteins in this region is believed to arise primarily from the heme group and the aromatic side chains (Chen et al., 1974; Sievers, 1978; Myer, 1985). At pH = 7.30, a prominent positive maximum position is seen at 262 nm associated with a huge negative ellipticity at 300 nm and a shoulder at 288 nm, which at very close to the previous published results (Sievers, 1978). Similar spectra were obtained at pH = 8.50 and pH = 9.70. The positive maxima shift from 262 to 253 nm (pH = 8.5) and 256 nm (pH = 9.7) and the negative shoulder at 288 nm (pH = 7.30) shifts, producing a single band at 280 nm for pH = 8.50 and bands at 275 and 284 nm at pH = 9.70.

The CD spectra of native CCP(II) in the far-UV region at alkaline pH are depicted in Figure 5A. The optical activity in this region can provide valuable information about the secondary and tertiary structure of proteins (Chen et al., 1974; Myer & Pande, 1976; Myer, 1985; Woody, 1985). The large negative signal at 210 nm with a shoulder at 220 nm shifts to 213 nm with its shoulder at 222 nm, with increasing ellipticities, while buffer pH raises from 7.30 to 9.70. It is also clear that changes in this portion of the CD spectrum occur between pH 8.50 and pH 9.70.

The pH dependence of the CD spectra (see Figure 5C) of CCP(II) in the Q-band region correlate well with the absorption data in regard to both the spin state and coordination number of the heme. At pH = 7.30, CCP(II) exhibits negative peaks at 590, 560, and 524 nm. These are typical of pentacoordinate high-spin hemes. At high pH values (8.50 and 9.70), sharper bands of negative ellipticity are evident at 557 nm (Q_0) and 540 nm (Q_1). There is a small decrease in ellipticity for the pH = 9.70 species. It is noteworthy that the Q-band ellipticities of CCP(II) bound to imidazole (spectrum not shown) more closely resemble those of the pH = 8.50 species.

It is apparent in Figure 6A that the absorption maxima (See Figure 1A) and the extrema of the CD spectra coincide very well (for all the pH conditions) in the Soret region (380–480 nm). The negative CD signals at 443 nm (pH = 7.30), 430 nm. (pH = 8.50), and 429 nm (pH = 9.70) correspond to the electronic transitions at 440 nm (pH = 7.30), 428 nm (pH = 8.50), and 426 nm (pH = 9.70). However, the CD spectra of the pH titration (from 7.30 to 9.70) do not exhibit the simple behavior predicted by a single high spin to low spin conversion. There is no doubt that the decrease in negative ellipticity at 443 nm corresponds to the dissappearance of high-spin heme as the pH is elevated. A plot of θ_{443} vs pH (Figure 6B) follows a titration curve consistent with the a pK_a of ~7.70. In contrast, growth of CD intensity from low-spin heme (at 430 nm) does not exhibit such simple behavior. Both the "low-spin" ellipticity and the integrated area of the CD signal cannot be modeled using a single low-spin heme species. Clearly, at pH values above ~8.50, the molar ellipticity of the low-spin species increases (since for pH ≥ 8.50 the fractional population of low-spin species is approximately constant).

Investigation on the Photolability of the High-pH, Low-Spin Heme. Ferrocytochrome *c* peroxidase was also examined in the pH region from 7.30 to 9.70, using much higher laser fluxes

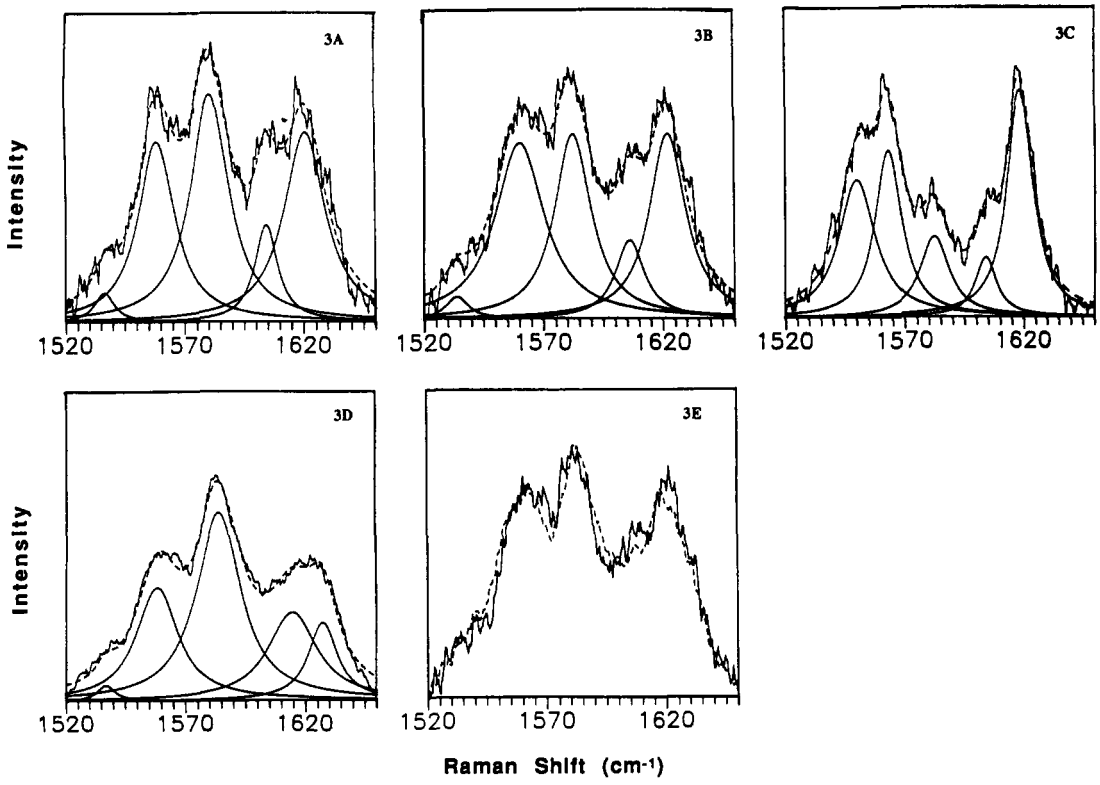

FIGURE 3: Deconvolution (A–D) and convolution (E) of resonance Raman spectra of fresh CCP(II) and its Imd derivative in 1520–1650 cm^{-1} (see Table III and text for details). Experimental data were obtained at low laser flux in 100 mM Tris-HCl buffer. (A) CCP(II), pH = 9.70; (B) CCP(II), pH = 8.50; (C) CCP(II), pH = 7.30; (D) CCP(II)–Imd (1:1), pH = 7.30. Dashed and solid lines represent the overall and individual curve-fit data, respectively. (E) Comparison of experimental data (solid line) obtained at pH = 8.50 with the convolution of the spectra of CCP(II) at pH = 7.30 (25%) and CCP(II)–Imd (75%) (dashed line).

(spherical optics without neutral density filters) to investigate the photolability of low-spin heme. Transient (10-ns) resonance Raman spectra recorded at pH = 7.60, 8.50, and 9.70 under high flux conditions are shown in parts A, B, and C of Figure 4, respectively. The spectra obtained at pH 7.60 were quite insensitive to laser flux. No evidence of photodegradation or phototransient heme species was found. In particular, the ratio of ν_3 intensity at 1471 cm^{-1} (pentacoordinate high spin) and at 1495 cm^{-1} (hexacoordinate low spin) was not dependent upon laser flux. As the pH was raised above pH = 7.60, the behavior of ν_3 showed a definite power dependence. The intensity at 1471 cm^{-1} increased relative to the intensity at 1495 cm^{-1} as a function of laser flux. This effect was entirely reversible (see Figure 7). The behavior of ν_3 is most easily rationalized as resulting from the photolysis of the strong field ligand which coordinates to the heme in the resting ferrous enzyme under alkaline conditions. Interestingly, at much higher pH values (pH > 9.2), little or no flux dependence was exhibited by ν_3.

A better illustration of the pH dependence of the photolysis extent of the low-spin species of alkaline CCP(II) is given in Figure 4D, where the photolysis extent is expressed in terms of the increase of the relative population of the high-spin species by the laser power increase. For instance, at pH 8.50, the fractional population of pentacoordinate high-spin species (ν_3 at 1471 cm^{-1}) increased from ~24% to ~50% as the laser flux was increased from 3×10^6 W/cm^2 to 1×10^8 W/cm^2. Apparently, the photodissociation yield of its axial low-spin ligand increases from pH = 7.60, maximizes at pH = 8.50, and finally vanishes at approximately pH = 9.20 (see Figure 4D).

Discussion

During the past two decades, it has become increasingly apparent that the functional properties of heme prosthetic groups are profoundly influenced by the architecture of their local protein environment. This is particularly true of ligand-binding proteins (such as hemoglobins and myoglobins) and several classes of catalytic heme proteins (oxidases and peroxidases). The protein environment can exercise at least two different levels of control over the heme active site. Its most direct influence comes in the form of the axial ligands it supplies. The number and identity of these ligands determine, to the first order, many of the heme's important functional properties (redox potential, affinity for exogenous ligands, chemical reactivity). More global changes in protein structure can also modulate function at the heme site by altering the tertiary structure of the heme pocket. In particular, the overall superstructure of the active site in CCP appears to be dependent upon hydrogen-bonding and nonbonding interactions on both the proximal (Asp-235 to Asn, Trp-191 to Phe) and distal (Trp-51 to Phe, Arg-48 to Leu and Lys) sides of the heme. The key role that Asp-235 plays in the hydrogen-bond network on the proximal side of ferrous peroxidase is evident by the downshift of ν_{Fe-His} from 240 cm^{-1} (for H-bonded imidazole) to 205 cm^{-1} (in neutral pH), typical of non-H-bonded imidazole (Smulevich et al., 1988a, 1989a). Other residues (e.g., Arg-48, Trp-191, and Trp-51) also participate, to varying extents, in forming the H-bond network inside the heme pocket to ferrous enzyme, as a low-spin form is observed for those mutants at high pH. Moreover, the breakdown of the H-bond network on the proximal side upon the replacement of Asp-235 by Asn observed for CCP(II) also takes place for its ferric form (Smulevich et al., 1988a; Satterlee et al., 1990). The CD and optical absorption data obtained in this study clearly show that pH-dependent changes occur both globally and locally heme environment. These, in

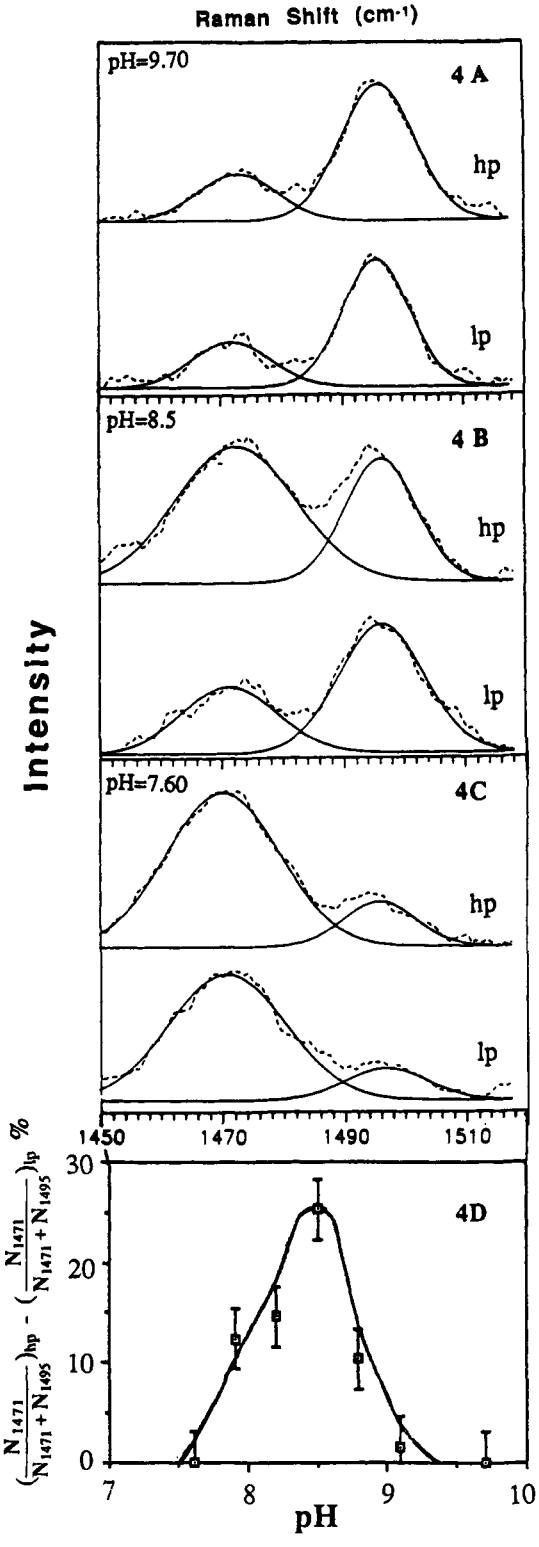

FIGURE 4: Resonance Raman spectra of fresh cytochrome c peroxidase (II) (100 mM Tris-HCl buffer) in the ν_3 region obtained at high and low fluxes: pH = 9.70 (A); pH = 8.50 (B); and pH = 7.60 (C). Dashed and solid lines represent the experimental and the curve-fit data, respectively. The spectra are sums of 10–15 scans recorded at 15 cm^{-1}/min, with the excitation wavelength at 436 nm. High power (hp): 7mW of power with a spherical optics ($\sim 1 \times 10^8$ W/cm^2). Low power (lp): 0.4-unit neutral density filter over 7 mW of power with a cylindrical optics ($\sim 3 \times 10^6$ W/cm^2). (D) The extent of low-spin ligand photolysis is expressed in terms of $[N_{1471}/(N_{1471} + N_{1495})]_{hp} - [N_{1471}/(N_{1471} + N_{1495})]_{lp}$ vs pH of buffers, where N_{1471} and N_{1495} represent the fractional populations of the "high-spin" and "low-spin" species, respectively, which have been corrected for relative resonance Raman cross-sections (see text for details).

Table II: Assignments of High-Frequency Resonance Raman Bands of CCP(II) at pH = 8.50 (Low Flux)

1360 (vs)	mixture of ν_4 (ls) and ν_4 (hs)	1583 (s)	ν_2 (ls)[a] + ν_{37} (hs)
1471 (w)	ν_3 (hs)	1606 (m)	ν_{37} (ls)[a] + ν_{10} (hs)
1495 (m)	ν_3 (ls)	1620 (s)	ν_{10} (ls)[a] + ν_{vinyl} (hs)
1560 (s)	ν_2 (hs)[a] + ν_{11} (hs) + ν_{11} (ls)	1629 (w)	ν_{vinyl} (ls)

[a] Donates the dominate contributions to the observed composite band.

turn, affect the photodynamics of the active site in fundamental ways.

Equilibrium Low-Spin Species of Ferrous CCP. All of the spectroscopic data collected in this study are consistent with a kinetically slow ($\tau_{1/2} > 1$ h) pH-dependent change in the equilibrium structure of the active site of ferrous CCP. This behavior is most evident in the absorption and CD spectra in the conversion of the heme from a high-spin to a low-spin species. Our data corroborate previous observations that the spin-state transition titrates with a pK_a between 7.5 and 8.0 (Conroy et al., 1978; Smulevich et al., 1989b). In our hands this phenomenon is reversible up to pH $\sim$ 10.0, whereupon the protein irreversibly denatures. The aging of ferric CCP first observed by Rousseau and co-workers (Dasgupta et al., 1989) does not appear to be a factor in the pH dependence of ferrous CCP.

Under pH = 8.50 conditions, CCP(II) exists as a mixture of high-spin and low-spin species. The resonance Raman spectra are particularly useful in characterizing this equilibrium. The cleanest separation of low-spin and high-spin bands occurs in the ν_3 region (1450–1520 cm^{-1}). Due to the very large relative cross-section (see Results section) of high-spin ν_3, its intensity remains quantifiable even when the fraction of high-spin species drops below 20% (see Figure 2B). The spectral region from 1520 to 1650 cm^{-1} is more complicated. However, a comparison of the spectra obtained from nearly pure high-spin (native ferrous CCP at pH = 7.30) and low-spin (ferrous CCP–Imd at pH – 7.30) samples coupled with a curve-fitting analysis allows for the assignment of all the major features of the high-frequency spectrum of CCP(II) at pH = 8.50 (see Table II). Because of resonance conditions, scattering from low-spin species tends to dominate the spectrum in this region. At pH = 9.70, contributions from the low-spin species are more prevalent, especially in the 1520–1650-cm^{-1} region (see Figure 2A).

It is of considerable interest to identify and characterize the ligand responsible for the alkaline spin-state transition in ferrous CCP. The resonance Raman and absorption spectra of CCP(II) at pH 8.50 clearly indicate that this ligand is a strong-field σ donor. The titration behavior of CCP(II) is, however, not consistent with the binding of an exogenous OH^-. First, the pK_a of the heme high spin to low spin transition is too low. More convincingly, both the Soret oscillator strength and the ellipticity of the Soret CD for ferrous CCP at pH 8.50 are relatively small for a six-coordinate low-spin heme (Sievers, 1978). This is suggestive of a relatively symmetrical disposition of axial ligands and contrasts dramatically with the spectra of CCP(II) bound to CN^- or other small exogenous ligands (see Figure 6). Moreover, the absorption, resonance Raman, and especially the CD data show no evidence for wholesale denaturation of the protein. This coupled with the complete reversibility of the spin-state transition suggests that there is no gross rearrangement of the amino acid residues in close proximity to the heme. Finally, it is noteworthy that approximately one-fifth of the hemes remains high spin even at pH $\geq$ 8.50. This behavior is inconsistent with the heme spin-state conversion being directly predicted upon the deprotonation of a potential sixth ligand. Instead, it is suggestive

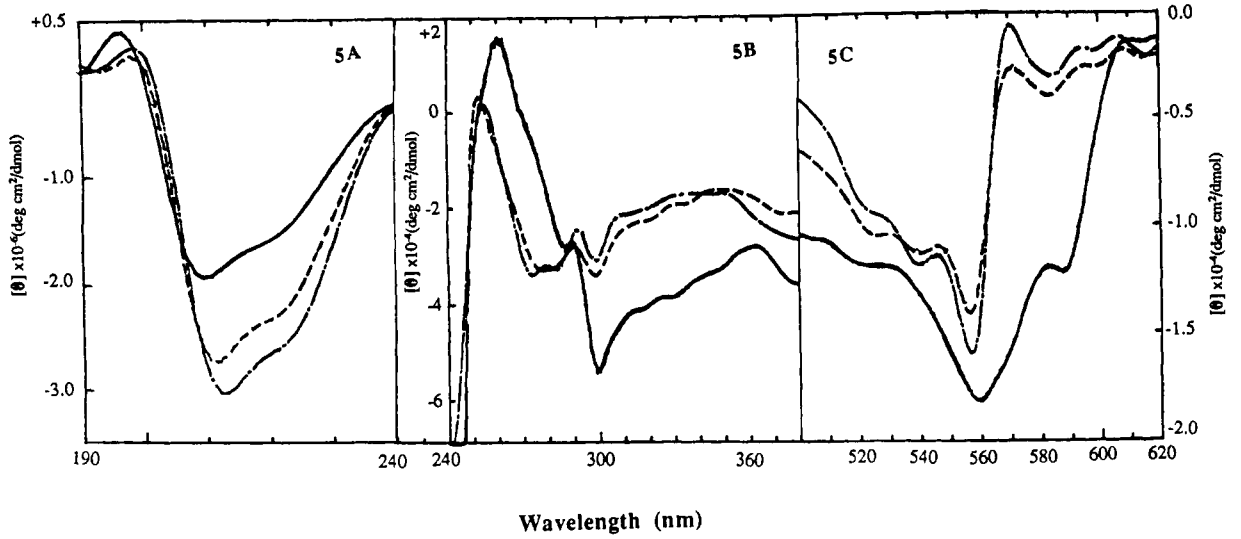

FIGURE 5: Circular dichroism spectra of fresh cytochrome *c* peroxidase (II) in the far-UV (A), near-UV (B), and visible (C) regions. A 200 mM Tris-HCl buffer was used at pH = 7.30 (—), pH = 8.50 (---), and pH = 9.70 (-·-). Spectra are corrected for background and represent the average of 10–20 scans recorded at 10 nm/min.

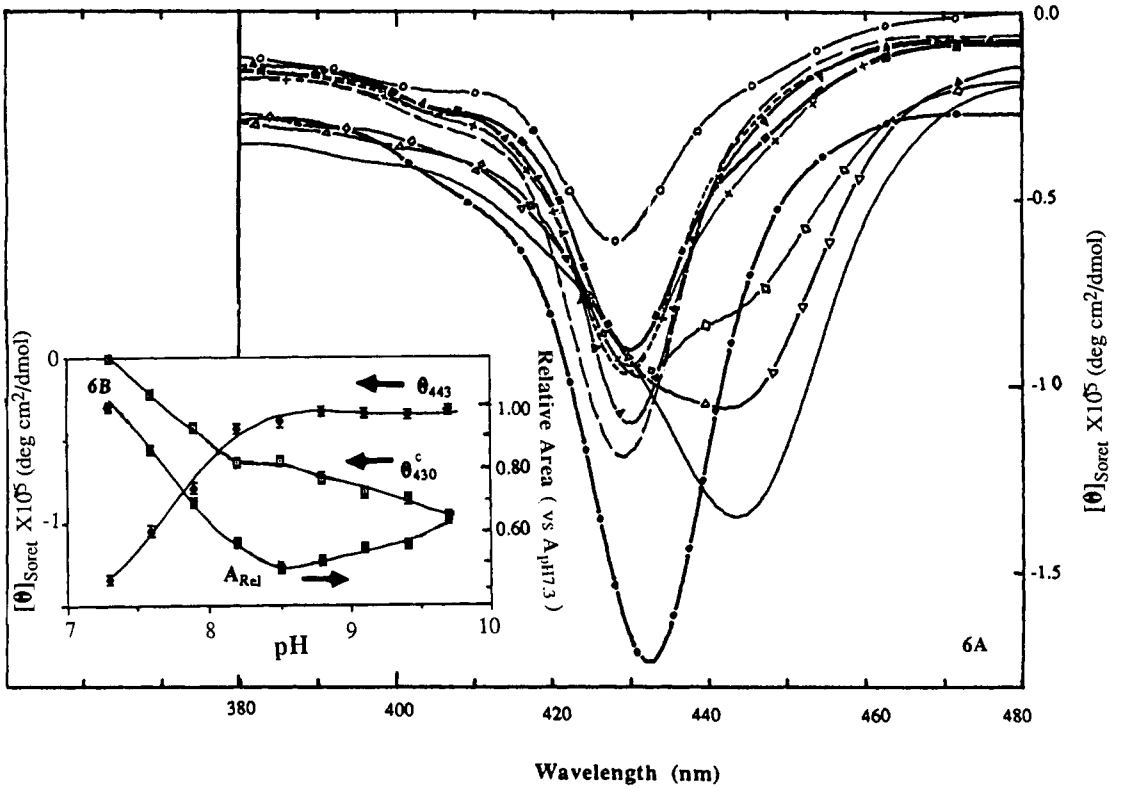

FIGURE 6: Circular dichroism spectra of fresh cytochrome *c* peroxidase (II) and its CN^- and imidazole derivatives in the Soret region (A). A 200 mM Tris-HCl buffer was used for CCP(II) at pH = 7.30 (—), pH = 7.60 (△), pH = 7.90 (◇), pH = 8.20 (+), pH = 8.50 (■), pH = 8.80 (---), pH = 9.40 (▲), pH = 9.70 (--), and its CN^- (●) and imidazole (1:1) (○) derivatives at pH = 7.30. Spectra are the average of eight scans recorded at 10 nm/min. (B) is a plot of the ellipticity changes of CCP(II) at 443 and 430 nm and the variation of relative area (vs that obtained at pH = 7.30) as a function of pH. The ellipticity at 430 nm contains contribution from high-spin heme. Therefore, the corrected ellipticity $[\theta^c_{430}(ls)]$ of low-spin heme at 430 nm is calculated by subtracting the contribution of high-spin heme from the original ellipticity (θ_{430}) at this wavelength.

$$\theta_{430}(hs) = \frac{\theta_{430}(100\%\ hs\ at\ pH = 7.30)}{\theta_{443}(100\%\ hs\ at\ pH = 7.30)}\theta_{443} = 0.6928\theta_{443} \quad (1)$$

$$\theta^c_{430}(ls) = \theta_{430} - \theta_{430}(hs) = \theta_{430} - 0.6928\theta_{443} \quad (2)$$

of structural alterations in the heme pocket which produce a thermal equilibrium between high-spin and low-spin species. On the basis of these considerations, we conclude that the sixth ligand bonding to the heme in alkaline CCP is a relatively nearby amino group in the distal pocket, most probably the imidazole of His-52.

pH Dependence of Equilibrium Low-Spin Species of Ferrous CCP. The optical spectra of equilibrium alkaline CCP(II) offer convincing evidence that changes continue to occur in the heme pocket at pH values well above the pK_a of the initial high spin to low spin transition. For instance, the absorption and CD spectra of CCP(II) at pH = 9.70 are quite distinct

Table III: Deconvolution of High-Frequency Bands of CCP(II) at Alkaline pH

	hs(CCP), pH = 7.30		ls(CCP), pH = 8.50		ls(CCP), pH = 9.70		ls(CCP/Imd), pH = 7.30	
modes (cm^{-1})	Raman shift	Γ	Raman shift	Γ	Raman shift	Γ	Raman shift	Γ
ν_{11}	1550.5	18.5	1560	22.5	1558	18.5	1558.5	21
ν_2	1563.5	13.5	1582.5	19.5	1580.5	19.5	1584	22
ν_{37}	1582.5	15	1606	14	1604	12		
							1614.5[a]	25
ν_{10}	1604	11						
			1622[a]	19	1620.5[a]	21		
$\nu_{C=C}$	1618.5	13					1627	15

[a] Not resolved in deconvolution.

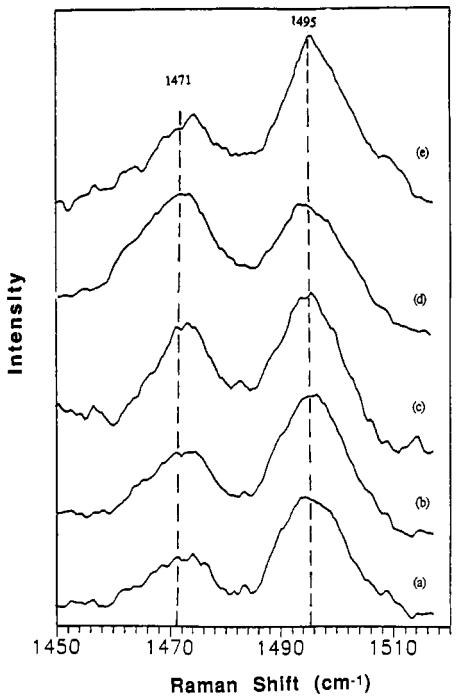

FIGURE 7: Resonance Raman spectra of cytochrome *c* peroxidase(II) in ν_3 region obtained at pH = 8.50 (100 mM Tris-HCl buffer). The spectra are sums of 10–15 scans recorded at 15 cm^{-1}/min, with the excitation wavelength at 436 nm: (a), 0.4-OD neutral density filter with cylindrical optics (flux = 3×10^6 W/cm^2); (b), same as (a) except 0.2-OD filter (flux = 5×10^6 W/cm^2); (c), no neutral density filter (flux = 8×10^6 W/cm^2); (d), spherical optics without neutral density filter (flux = 1×10^8 W/cm^2); (e), same as (a), recorded immediately after the measurement of spectrum d.

from those of pH = 8.50 species. Both the extinction coefficient and the ellipticity of the Soret band grow as the pH is increased from 8.50 to 9.70 in a manner disproportionate with the rather modest increase in the fraction of low-spin hemes. Furthermore, the titration behavior of the Soret band CD (see Figure 6B) and ν_3 in the resonance Raman spectra, while consistent with the disappearance of a single high-spin species, cannot be modeled by the appearance of only a single low-spin species. The titration curve in Figure 2B is quite asymmetric, indicating the possible existence of a second ionizable group at pH > 7.70. Spectrophotometric titrations obtained immediately after pH changes (Conroy et al., 1978) indicate a cooperative two-proton ionization which probably involves His-181 (Miller et al., 1990). Since our data were obtained under equlibrium conditions, perhaps this cooperative ionization is resolved into two single ionizations.

The near-UV (240–380-nm) and far-UV (190–240-nm) regions of protein CD spectra have long been known to be quite sensitive to the local environment of aromatic residues, (and heme tertiary structure) and the secondary structures of proteins, respectively (Chen et al., 1974; Myer, 1985; Woody, 1985). The CD spectra of CCP(II) in the far UV (Figure 5A) and near UV (Figure 5B) demonstrate that significant changes in protein tertiary and secondary structures occur coincident with the spin-state change at the heme. They also show that global protein changes continue to occur as the pH is raised further. These perturbations are undoubtedly propagated to the heme pocket causing the pH-dependent alterations in the low-spin heme absorption and CD spectra.

Interestingly, these perturbations apparently have little further effect upon the high spin/low spin equilibrium. In fact, the high-frequency resonance Raman spectrum of equilibrium CCP(II) reveal little or no significant differences in the geometry of the heme itself between pH 8.50 and pH 9.70 species. Deconvolution of the 1500–1650-cm^{-1} region of the spectra yields approximately the same positions and line widths for low-spin heme bands irrespective of pH (see Table III). Although the S/N of the spectra are insufficient to yield unique quantitative fits (see Results), it is clear that there are no dramatic changes in either heme core size or planarity in the low-spin species as a consequence of increasing the pH. Nonetheless, the low-spin species at pH 8.50 and 9.70, respectively, are functionally different. Previous studies by Erman and co-workers have demonstrated significant differences in the reduction potential of CCP in this pH range (Conroy et al., 1978). Furthermore, the transient resonance Raman spectra obtained in this study show a dramatic difference in the photodynamics of low-spin CCP(II) as a function of pH (see discussion below). We conclude that the distinctions between low-spin CCP(II) species lie in the interactions between the heme and the strong-field axial ligand (His-52) which becomes accessible to the heme under alkaline conditions.

In an effort to further characterize the equilibrium heme pocket structures of alkaline CCP(II), we prepared the imidazole adduct of CCP(II) at pH = 7.30. This readily produced a low-spin heme species, indicating that the distal heme pocket is quite spacious as expected from the results of X-ray crystallographic studies. The low-spin heme of CCP(II)–imidazole exhibits relatively low values for both the extinction coefficient and the ellipticity of the Soret band. This is consistent with a fairly symmetric axial ligation environment of the heme. It is interesting to note that this heme–imidazole site more closely resembles the low-spin CCP(II) species at pH = 8.5 than CCP(II) at pH = 9.70. This suggests that the distal pocket geometry is altered at the higher pH in a manner that distorts the axial symmetry of the low-spin heme complex. We speculate that conformational changes in the distal pocket directly affect either the bond length or angle between the heme and His-52.

Photodynamics of CCP(II). The dynamics of ligand photolysis and rebinding in heme proteins has recently become an area of increasing interest. To date, most spectroscopic investigations have focused upon the photolytic behavior of small exogenous, π-bonding ligands (CO, NO, O_2, etc.) (Spiro, 1987; Findsen et al., 1987; Rousseau & Friedman, 1988;

Findsen & Ondrias, 1990, and references therein). Time-resolved studies of nickel porphyrins have shown that nitrogenous ligands are readily photolyzed from those species (Kim & Holten, 1983; Findsen et al., 1986; Crawford et al., 1988, and references therein). Photolability of endogenous ligands in hexacoordinate heme systems has, however, only rarely been observed. Jongeward et al. (1988) have observed ligand photolysis and recombination in cytochrome b_5 and c on picosecond time scales. Ligation and subsequent photolysis of an endogenous ligand has been postulated to occur following CO photolysis in fully reduced cytochrome c oxidase (Woodruff et al., 1991). Finally, Spiro and co-workers (Smulevich et al., 1989b) have recently found evidence for ligand photolysis in high-power steady-state spectra of low-spin CCP(II). The new data obtained in this study suggest that the photolability of strong-field σ ligands may be significantly altered by relatively subtle changes in the local heme–ligand environment.

The time resolution of the present investigation offers new insights into the dynamics of ligand photolysis in low-spin CCP(II). At pH 8.50, photolysis is quite efficient. It occurs rapidly (within the 10-ns laser pulse width) and with relatively high yield. Moreover, it is completely reversible. While the lifetime of ligand recombination is sufficiently long for the pentacoordinate photolyzed heme to be apparent within the pump pulse, religation kinetics are rapid enough for protein relaxation to the hexacoordinate ground state to occur between laser pulses (<50 ms). It should be noted that the spectra obtained with the single-pulse protocol of this study are transient (as opposed to time-resolved) spectra and therefore represent the photoresponse of CCP(II) integrated over the 10-ns pulses as opposed to the steady-state conditions generated by CW irradiation in previous studies (Smulevich et al., 1989b). Since the sample is being continuously pumped while the RRS is generated, the 10-ns pulse width does not represent either an upper or lower bound for the transient in the species lifetime. However, the appearance of a photolyzed heme transient in the spectra does indicate that its rise time is quite short relative to both its lifetime and the laser pulse width. We speculate that the rise time for ligand photolysis is very rapid (<nanosecond) by analogy to the behavior of nickel porphyrins (Kim & Holten, 1983; Findsen et al., 1986; Crawford et al., 1988, and references therein) and cytochromes b_5 and c (Jongeward et al., 1988). It is the relatively long half-life of the photolytic transient that allows its detection in nanosecond pulses and under high-power steady-state illumination. Indeed, true time-resolved data (not shown) suggest that the half-life of the photolyzed hemes (at pH 8.50) is ≥500 ns (Wang et al., 1992).

The transient high-spin heme species generated by ligand photolysis at pH 8.50 is structurally quite similar to the equilibrium high-spin species. Spectral deconvolution of the "high-flux" transient resonance Raman spectra (data not shown) reveals no significant shifts (<2 cm^{-1} under our conditions) in either ν_4 or the core-size marker bands. This behavior contrasts with that of carbonmonoxyhemoglobins and CO-bound cytochrome oxidase, which display metastable heme pocket geometries about the high-spin heme subsequent to ligand photolysis (Findsen et al., 1987). Thus, it is likely the CCP(II) does not undergo a large-scale rearrangement of protein tertiary structure as a result of binding the endogenous sixth ligand. These data also strongly suggest that the proximal histidine-175 is not the photolabile ligand.

Interestingly, the pH-induced changes in heme environment seem to be localized in the heme–imidazole bonding interactions since no large structural perturbations of the heme itself are observed in raising the pH from 8.50 to 9.70. Nonetheless, those environmental perturbations have a profound effect on ligand photolability. This may have general relevance to the photodynamics of six-coordinate hemes with σ ligands. We speculate that any of three scenarios may produce the pH-dependent photodynamic behavior of CCP(II). The efficiency of photolysis may be affected in either of the two ways: (1) changes in the heme–His-52 geometry or (2) changes in the protonation state of His-52. The CD and UV/vis data suggest that upon raising the pH to 9.70, the local heme environment becomes less symmetric (see above). This distortion might represent relatively large changes in heme–histidine bond angle or bond length. The photodissociative process (by analogy to either CO photolysis from heme proteins or nitrogenous base photolysis from nickel porphyrins) undoubtedly involves either C–T or d–d states which lie below the Soret transition. Coupling between the singlet excited state generated by near-UV pumping and these dissociative states would be expected to depend strongly on heme–ligand geometry. Similar effects have been noted for Hb–CO and hexacoordinate nickel corphinoids. Alternatively, the protonation state of the sixth ligand might influence the excited-state dynamics. The pK_a for His-52 can be reasonably expected to lie between 7.0 and 9.0. Moreover, protonation of His-52 would also alter the ligand symmetry of the hexacoordinate heme and thus account for the CD and UV/vis data. However, if this were true, it is likely that the net high spin/low spin equilibrium would be affected. Furthermore, the pH dependence of ligand photolysis would be expected to display monotonic behavior typical of a titration instead of peaking at pH ~ 8.50. For these reasons, we believe that this scenario is less likely than the first. Finally, the low photolysis yield within the 10-ns probe pulse at pH = 9.70 might result from more rapid heme–ligand recombination instead of changes in instrinsic yield. Similar behavior is seen in cytochrome c and b_5 (Jongeward et al., 1988) and accounts for a large portion of the difference in net quantum yield between O_2 and CO photolysis in globins (Rousseau & Friedman, 1988; Findsen & Ondrias, 1990, and references therein). The present data cannot exclude this possibility. Photolysis experiments conducted on picosecond time scales are necessary in order to fully resolve the photodynamics of ferrous CCP.

Conclusions

The present work expands upon previous studies of alkaline ferrous CCP by quantifying the titration behavior of the enzyme under equilibrium conditions. In addition, CD and transient resonance Raman spectroscopy were employed for the first time to characterize both the equilibrium and dynamic behavior of multiple low-spin species formed at elevated pH values (7.90–9.70) and imidazole adducts of CCP(II) used to model these species. Our data offer several new insights into the effects of global protein perturbations on the structure and dynamics of the heme environment of ferrous CCP.

(1) CCP(II) undergoes a relatively slow, time- and temperature-dependent spin-state transition (from 5 c/hs to 6 c/ls) when exposed to alkaline media, producing a low-spin spectrum identical to that of its imidazole derivative. The low-spin species of alkaline CCP(II) is fairly stable (at least 6–8 h, 4 °C) under laser irradiation.

(2) A pH titration monitored by resonance Raman displays an asymmetric curve, with pK_a = 7.70, suggesting that more than one ionization group participated in the heme spin-state transition. A small amount of high-spin species remains present at pH 9.70, indicating that even under these conditions an equilibrium exists between high- and low-spin forms.

(3) The reversible photolability of the low-spin heme of alkaline CCP(II) is quite pH dependent, showing the maximum photolysis yield at pH ~ 8.50. In contrast, its imidazole derivative is not photolabile.

(4) At least two low-spin species of CCP(II) can be observed under alkaline conditions. Both the heme pocket structure (as evidenced by the CD spectra) and the photolysis behavior of the heme, observed in the transient resonance Raman spectra, vary substantially as the pH is raised from 8.50 to 9.70.

Added in Proof

Subsequent to the submission of the manuscript, Smulevich et al. (1991) published a resonance Raman study of pH-induced conformational changes in equilibrium ferric, ferrous, and CO-ferrous forms of site-directed mutants of CCP. Their results showed that His-52 is the likely sixth ligand in alkaline CCP(II). They further concluded that protein conformational changes controlled the heme chemistry.

Acknowledgments

We gratefully acknowledge J. Satterlee, J. Erman, S. Moench, and R. Larsen for stimulating and helpful discussions, and we especially thank S. Moench and H. Zhu for their help with our initial CCP preparations. The financial support of the National Institutes of Health (GM33330) is also acknowledged.

References

Chen, Y.-H., Yang, J. T., & Chau, K. H. (1974) *Biochemistry 13* (6), 3350–3359.

Conroy, C. W., Tyma, P., Daum, P. H., & Erman, J. E. (1978) *Biochim. Biophys. Acta 537*, 62–69.

Crawford, B. A., Findsen, E. W., Ondrias, M. R., & Shelnult, J. A. (1988) *Inorg. Chem. 27*, 1842–1846.

Dasgupta, S., Rousseau, D. L., Anni, H., & Yonetani, T. (1989) *J. Biol. Chem. 264* (1), 654–662.

Dowe, R. J., & Erman, J. E. (1985) *Biochim. Biophys. Acta 827*, 183–189.

Erman, J. E., Vitello, L. B., Mauro, J. M., & Kraut, J. (1989) *Biochemistry 28* (20), 7992–7995.

Evangelista-Kirkup, R., Crisanti, M., Poulos, T. L., & Spiro, T. G. (1985) *FEBS Lett. 190* (2), 221–226.

Felton, R. H., Romans, A. Y., Yu, N.-T., & Schonbaum, G. R. (1976) *Biochim. Biophys. Acta 434*, 82–89.

Findsen, E. W., & Ondrias, M. R. (1990) *Photochem. Photobiol. 51* (6), 741–748.

Findsen, E. W., Alston, K., Shelnult, J. A., & Ondrias, M. R. (1986) *J. Am. Chem. Soc. 108*, 4009–4017.

Findsen, E. W., Centeno, J., Babcock, G. T., & Ondrias, M. R. (1987) *J. Am. Chem. Soc. 109* (18), 5367–5372.

Goodin, D. B., Mauk, A. G., & Smith, M. (1987) *J. Biol. Chem. 262* (16), 7719–7724.

Hashimoto, S., Teraoka, J., Inubushi, T., Yonetani, T., & Kitagawa, T. (1986) *J. Biol. Chem. 261* (24), 11110–11118.

Jongeward, K. A., Magda, D., Taube, D. J., & Traylor, T. G. (1988) *J. Biol. Chem. 263* (13), 6027–30.

Kang, C. H., Ferguson-Miller, S., & Margoliash, E. (1977) *J. Biol. Chem. 252*, 919–926.

Kim, D. H., & Holten, D. (1983) *Chem. Phys. 75*, 305–312.

Larsen, R. W. (1990) Ph.D. Dissertation, University of New Mexico.

Miller, M. A., Coletta, M., Mauro, J. M., Putnam, L. D., Farnum, M. F., Kraut, J., & Traylor, T. G. (1990) *Biochemistry 29* (7), 1777–1791.

Moench, S. J. (1986) Ph.D. Dissertation, Colorado State University.

Myer, Y. P. (1985) in *Curr. Top. Bioenerg. 14*, 149–188.

Myer, Y. P., & Pande, A. (1976) in *The Porphyrins* (Dolphin, D., Ed.) Vol. III, pp 271–322, Academic Press, New York.

Nelson, C. E., Sitzman, E. V., Kang, C. H., & Margoliash, E. (1977) *Anal. Biochem. 83*, 622–631.

Poulos, T. L. (1982) in *Electron Transport & Oxygen Utilization* (Ho, C., et al., Eds.) pp 217–221, Elsevier North Holland Inc., New York.

Poulos, T. L., & Finzel, B. C. (1984) *Pept. Protein Rev. 4*, 115–171.

Poulos, T. L., Freer, S. T., Alden, R. A., Edwards, S. L., Skogland, U., Takio, K., Eriksson, B., Xuong, N., Yonetani, T., & Kraut, J. (1980) *J. Biol. Chem. 255* (2), 575–580.

Reczek, C. M., Sitter, A. J., & Terner, J. (1989) *J. Mol. Struct. 214*, 27–41.

Rousseau, D. L., & Friedman, J. M. (1987) in *Biological Applications of Raman Spectroscopy* (Spiro, T. G., Ed.) Vol. III, pp 133–213, Wiley, New York.

Satterlee, J. D., Erman, J. E., Mauro, J. M., & Kraut, J. (1990) *Biochemistry 29* (37), 8797–8804.

Shelnutt, J. A., Satterlee, J. D., & Erman, J. E. (1983) *J. Biol. Chem. 258* (4), 2168–2173.

Sievers, G. (1978) *Biochim. Biophys. Acta 536*, 212–225.

Sievers, G., Osterlund, K., & Ellfolk, N. (1979) *Biochim. Biophys. Acta 581*, 1–14.

Sivaraja, M., Goodin, D. B., Smith, M., & Hoffman, B. M. (1989) *Science 245*, 738–740.

Smulevich, G., Dasgupta, S., English, A., & Spiro, T. G. (1986a) *Biochim. Biophys. Acta 873*, 88–91.

Smulevich, G., Evangelista-Kirkup, R., English, A., & Spiro, T. G. (1986b) *Biochemistry 25* (15), 4426–4430.

Smulevich, G., Evangelista-Kirkup, R., English, A., & Spiro, T. G. (1986c) *J. Mol. Struct. 141*, 411–414.

Smulevich, G., Mauro, J. M., Fishel, L. A., English, A. M., Kraut, J., & Spiro, T. G. (1988a) *Biochemistry 27* (15), 5477–5485.

Smulevich, G., Mauro, J. M., Fishel, L. A., English, A. M., Kraut, J., & Spiro, T. G. (1988b) *Biochemistry 27* (15), 5486–5492.

Smulevich, G., Mantini, A. R., English, A. M., & Mauro, J. M. (1989a) *Biochemistry 28* (12), 5058–5064.

Smulevich, G., Miller, M. A., Gosztola, D., & Spiro, T. G. (1989b) *Biochemistry 28* (26), 9905–9908.

Smulevich, G., Wang, Y., Edwards, S. L., Poulos, T. L., English, A. M., & Spiro, T. G. (1990) *Biochemistry 29* (10), 2586–2592.

Smulevich, G., Miller, M. A., Kraut, J., & Spiro, T. G. (1991) *Biochemistry 30*, 9546–9558.

Spiro, T. G. (1983) in *Fe-Porphyrines* (Lever, A. B. P., & Gray, H. B., Eds.) Part II, pp 89–160, Addison-Wesley, Massachusetts.

Spiro, T. G. (1985) *Adv. Protein Chem. 37*, 110.

Spiro, T. G. (1987) *Biological Applications of Raman Spectroscopy* (Spiro, T. G., Ed.) Vol. III, Wiley, New York.

Spiro, T. G., Smulevich, G., & Su, C. (1990) *Biochemistry 29* (19), 4497–4508.

Tsaprailis, G., Fox, T., English, A. M., Miller, M. A., & Kraut, J. (1991) *J. Inorg. Biochem. 43* (2–3), 339.

Wang, J., Larsen, R. W., & Ondrias, M. R. (1990) *Biophys. J. 57* (2), 236.

Wang, J., Boldt, N. J., & Ondrias, M. R. (1991) *J. Inorg. Biochem. 43* (2–3), 345.

Wang, J., Larsen, R. W., Chan, S. I., Boldt, N. J., & Ondrias, M. R. (1992) *J. Am. Chem. Soc.* (in press).

Wittenberg, B. A., Kampa, L., Wittenberg, J. B., Blumberg, W. E., & Peisach, J. (1968) *J. Biol. Chem. 243* (8), 1863-1870.
Woodruff, W. H., Einarsdottir, O., Dyer, R. B., Bagley, K. A., Palmer, G., Atherton, S. J., Goldbeck, R. A., Dawes, T. D., & Kliger, D. S. (1991) *Proc. Natl. Acad. Sci. U.S.A. 88*, 2588-2592.
Woody, R. W. (1985) in *The Peptides* (Udenfriend, S., & Meienhofer, J., Eds.) Vol. VII, pp 15-114, Academic Press, New York.
Yonetani, T. (1970) *Advances in Enzymology* (Nord, F. F., Ed.) Vol. 33, pp 309-335, Interscience, New York.
Yonetani, T. (1976) in *Enzymes (3rd Ed.)* (Boyer, P. D., Ed.) Vol. XIII, pp 345-361, Academic Press, New York.
Yonetani, T., & Ray, G. (1965) *J. Biol. Chem. 240* (11), 4503-4508.

Catalytic Sites of *Escherichia coli* F_1-ATPase. Characterization of Unisite Catalysis at Varied pH†

Marwan K. Al-Shawi and Alan E. Senior*
Department of Biochemistry, University of Rochester, School of Medicine and Dentistry, Rochester, New York 14642
Received August 20, 1991; Revised Manuscript Received October 17, 1991

ABSTRACT: Using manual rapid-mixing procedures in which small, equal volumes of *Escherichia coli* F_1-ATPase and [γ-^{32}P]ATP were combined at final concentrations of 2 and 0.2 μM, respectively (i.e., unisite catalysis conditions), it was shown that ≥66% of the ^{32}P became bound to the enzyme, with the ratio of bound ATP/bound P_i equal to 0.4 and the rate of dissociation of bound [^{32}P]P_i equal to 3.5×10^{-3} s^{-1}, similar to previously published values. Azide is known to inhibit cooperative but not unisite catalysis in F_1-ATPase [Noumi, T., Maeda, M., & Futai, M. (1987) *FEBS Lett. 213*, 381-384]. In the presence of 1 mM sodium azide, 99% of the ^{32}P became bound to the enzyme, with the ratio of bound ATP/bound P_i being 0.57. These experiments demonstrated that when conditions are used which minimize cooperative catalysis, most or all of the F_1 molecules bind substoichiometric ATP tightly, hydrolyze it with retention of bound ATP and P_i, and release the products slowly. The data justify the validity of previously published rate constants for unisite catalysis. Unisite catalysis in *E. coli* F_1-ATPase was studied at varied pH from 5.5 to 9.5 using buffers devoid of phosphate. Rate constants for ATP binding/release, ATP hydrolysis/resynthesis, P_i release, and ADP binding/release were measured; the P_i binding rate constant was inferred from the ΔG for ATP hydrolysis. ATP binding was pH-independent; ATP release accelerated at higher pH. The highest K_a^{ATP} (4.4×10^9 M^{-1}) was seen at physiological pH 7.5. ATP hydrolysis and resynthesis were pH-independent, and the equilibrium constant for the cleavage/condensation reaction was around 2 at all pH values, showing catalysis occurred in a sequestered environment. P_i release was pH-independent, but P_i binding was drastically slowed at high pH. $K_d^{P_i}$, which was around 1 M at pH 5.5-7.5, reached 1.3×10^6 M at pH 9.5. ADP release was pH-independent; ADP binding was somewhat pH-sensitive, such that K_d^{ADP} decreased steadily from 42 μM at pH 5.5 to 430 nM at pH 9.5. The data confirm the view that, during normal oxidative phosphorylation, energy input from $\Delta\mu_{H^+}$ is required for P_i binding and ATP release. The data also support the idea that two major enzyme conformations are involved in unisite catalysis and that an ionic interaction influences binding of P_i and release of ATP in one conformation. In contrast to unisite ATP hydrolysis, multisite ATP hydrolysis was pH-dependent in the range pH 5.0-9.5, showing that the rate enhancements deriving from cooperative intersubunit interactions involve ionizable groups on the protein.

An important impetus for recent work on the mechanism of ATP synthesis by oxidative phosphorylation and photophosphorylation derived from the discovery of "unisite catalysis" in soluble F_1-ATPase from bovine heart mitochondria (Grubmeyer & Penefsky, 1981a,b; Grubmeyer et al., 1982). Unisite catalysis occurs when substrate ATP binds to a single site on F_1 and is characterized by (a) very high affinity binding of ATP, (b) reversible ($K_{eq} \sim 1$) hydrolysis and resynthesis of bound ATP to and from bound ADP and P_i, and (c) slow release of the products P_i and ADP. "Multisite catalysis", corresponding to V_{max} rates, occurs when two or three catalytic sites on F_1 are occupied by substrate and involves a large, positively cooperative acceleration of chemical catalysis and product-release rates (Cross et al., 1982). In more recent studies, Penefsky (1985a,b) demonstrated that unisite catalysis by bovine heart ATP synthase in membranes has similar characteristics to that of soluble F_1, and in response to questions regarding the significance of unisite catalysis in mitochondrial F_1 (Bullough et al., 1987), Penefsky (1988) and Cunningham and Cross (1988) demonstrated that unisite catalysis and its "promotion" to a multisite rate are a reflection of activity at a normal catalytic site. Unisite catalysis has been confirmed in F_1-ATPases from other sources including *Escherichia coli* (Wise et al., 1984) and yeast (Mueller, 1990), and Penefsky and Cross (1991) have recently reviewed the field. A scheme for unisite catalysis showing each of the four steps is

$$F_1 + ATP \underset{k_{-1}}{\overset{k_{+1}}{\rightleftharpoons}} F_1{<}ATP \underset{k_{-2}}{\overset{k_{+2}}{\rightleftharpoons}} F_1{<}ADP{\cdot}P_i \underset{k_{-3}}{\overset{k_{+3}}{\rightleftharpoons}}$$
$$F_1{<}ADP + P_i \underset{k_{-4}}{\overset{k_{+4}}{\rightleftharpoons}} F_1 + ADP$$

† This work was supported by NIH Grant GM25349 to A.E.S.

0006-2960/92/0431-878$03.00/0